Adaptive Controller Tuning Method Based on Online Multi-objective Optimization: A Case Study of the Four-bar Mechanism

Alejandro Rodríguez-Molina[1], Miguel G. Villarreal-Cervantes[1], Efrén Mezura-Montes[2], Mario Aldape-Pérez[1]

***Abstract*—The efficient speed regulation of four-bar mechanisms is required for many industrial processes. These mechanisms are hard to control due to the highly non-linear behavior and the presence of uncertainties or disturbances. In this work, different Pareto front approximation search approaches in the adaptive controller tuning based on online multi-objective meta-heuristic optimization, are studied through their application in the four-bar mechanism speed regulation problem. Dominance-based, decomposition-based, metric-driven and hybrid search approaches included in algorithms NSGA-II, MOEA/D-DE, SMS-EMOA, and NSGA-III, respectively, are considered in this study. Also, a proposed metric-driven algorithm based on the Differential Evolution and the hypervolume indicator (HV-MODE) is incorporated into the analysis. The comparative descriptive and non-parametric statistical evidence presented in this work shows the effectiveness of the adaptive controller tuning based on online multi-objective meta-heuristic optimization and reveals advantages of the metric-driven search approach.**

***Index Terms*—Meta-heuristics, multi-objective optimization, adaptive tuning, intelligent control, four-bar mechanism.**

I. Introduction

A. Background and context

Four-bar mechanisms (FBMs) conform to a particular class of closed kinematic chain mechanisms. These mechanisms can follow predefined non-linear planar trajectories with a single degree of freedom. They are widely used in several industrial applications due to their lower cost, higher precision when following a particular trajectory, greater force rates and simplicity compared with serial mechanisms. Nevertheless, the design of appropriate control strategies turns out to be difficult because these mechanisms have highly non-linear dynamics with behaviors that are difficult to govern. Moreover, if mechanisms are subject to uncertainties (such as load perturbations, unmodeled dynamics, and unfavorable operating environments), the design process of a suitable control strategy may be even harder.

In a general point of view, dynamic systems are required to have the desired behaviors to generate useful engineering applications. Control engineering is responsible for analyzing those systems and design suitable control strategies or controllers that properly govern their behaviors.

Some well classical controllers such as the linear [1] or model-based [2] ones have been used to control the speed of the FBM. These alternatives have a proven control performance but present some difficulties when there are uncertainties or disturbances.

On the other hand, the control system has a set of parameters that compromise their performance. The setting of these parameters, known as the tuning task, is one of the most important problems in control engineering. Depending on a selected parameter configuration, controllers can improve or diminish the closed-loop system accuracy, sensibility, robustness, energetic efficiency, and overall operation quality. Then, the controller tuning impacts in the productivity, production cost and product quality in the industry.

The controller tuning must be performed by considering a set of well-established performance requirements [3] to satisfy the necessities of modern applications, which use dynamic systems with increasing complexity. In most of the cases, there are several trade-offs among these requirements which make the tuning task a very complex problem.

Controller tuning approaches can be classified into four categories [4]:

- Analytical methods, which use tools from conventional classical and modern control theory to find the controller parameters by analyzing the closed-loop system stability.
- Heuristic methods, where the controller parameters are chosen manually based on empirical knowledge of the dynamic system behavior.
- Optimization tuning methods, in which a mathematical programming problem is stated and then is solved by an optimizer to find the most suitable controller parameters.
- Adaptive tuning methods that obtain the controller parameters online by using an identification process and a combination of the above methods. Unlike the rest of the tuning methods where the controller parameters remain fixed, in the adaptive approach, those parameters are updated continuously in response to the control system changes. This tuning approach is suitable for high precision control systems which are subject to unbounded uncertainties or disturbances.

Analytical and heuristic tuning methods cannot always satisfy more than one tuning criteria. Unlike these, optimization methods can consider several performance requirements at the same time by stating a multi-objective optimization

Alejandro Rodríguez-Molina at arodriguezm0902@alumno.ipn.mx
Efrén Mezura-Montes at emezura@uv.mx
Miguel G. Villarreal-Cervantes at Tel.: +52 55 57296000 and mvillarrealc@ipn.mx
Mario Aldape-Pérez at Tel.: +52 55 57296000 and mvillarrealc@ipn.mx
[1] Posgraduate Department, Instituto Politécnico Nacional, CIDETEC, Mexico city, 07700, Mexico.
[2] Artificial Intelligence Research Center, University of Veracruz, Xalapa Veracruz, 91000, Mexico

problem (MOP). Moreover, these can include computational intelligence techniques to handle the most complex tuning problems.

The use of computational intelligence in control engineering is commonly referred to as intelligent control [5] and has been increased in industrial problems where classical and modern control theory tuning approaches have not been proven to be successful enough [6].

Among computational intelligence techniques, meta-heuristics are alternatives that can find good solutions to very complex optimization problems at a reasonable computational cost [7]. Because of this, these techniques have been adopted in several optimization tuning methods for a wide variety of control engineering applications that require to fulfill a set of specifications stated as a MOP [8]. In [9] for example, the proportional, integral and derivative gains of two Proportional Integral Derivative (PID) controllers for a double pendulum are tuned by using the Non-dominated Sorting Genetic Algorithm II (NSGA-II) [10]. In this, the requirements are the minimization of the links position errors and the variation of the control signals. A multi-objective variant of the Particle Swarm Optimization (PSO) [11], named Ingenious-MOPSO, is employed in [12] to tune a sliding mode controller for a biped robot. This controller parameters include three positive constants and three sliding surfaces. The minimization of the robot angle errors and the control effort are considered as the tuning criteria. The work in [13] uses the Multi-objective Genetic Algorithm (MOGA) [14] over a grid computing environment to tune the weights of a loop-shaping H_∞ robust controller for a Boeing 747 aircraft. The tuned controller is used to decrease the over-shoot, settling-time and rise-time of the control system. PMODE, a Pareto based multi-objective variant of Differential Evolution (DE) [15], is used in [16] to tune the gains of a PID controller for a flexible link system. Five tuning requirements are considered in the MOP, the over-shoot, steady-state-error, system response, and maximum peak response. In [17], the number of inputs, membership functions, and fuzzy rules, as well as the and-or-ignore conjugates and the defuzzification algorithm are also tuned by MOGA for a DC motor. Real-time information of hardware in the loop simulation of the control system is used to measure the quality of a given configuration regarding the rise-time, steady-state-error, energy consumption, and implementation complexity. Another fuzzy controller is tuned in [18]. In this, the centers and widths of the Gaussian membership functions, the number of fuzzy control rules and the gains of a fuzzy PID controller are tuned by using a Genetic Algorithm (GA) [19] for a Pendubot system. A MOP that considers the minimization of the fuzzy rules numbers and the operation error is stated and then transformed to a single-objective problem through a preference-based method. In [20], a multi-objective external optimization approach is used to tune the gains and orders of the fractional order PID (FOPID) controller for an Automatic Voltage Regulator (AVR) to minimize the regulation and steady-state errors, as well as the settling time. A similar optimization approach is adopted in [21] to adjust the FOPID controller with the aim to improve the performance of an islanded microgrid and minimize the frequency deviation and the controller output signal.

For all the above works related to optimization tuning methods, the tuned controllers remain fixed. They show good performance when the controlled system is not subject to uncertainties or disturbances or when these last have bounded behaviors. Nevertheless, when these present large uncertainties, the good performance of the fixed controllers cannot be ensured, and the use of adaptive tuning methods is necessary.

Meta-heuristic multi-objective optimization approaches have also been adopted by adaptive tuning methods, i.e., the controller parameters are updated online through a multi-objective meta-heuristic optimization process. However, they have been less explored despite their possible advantages in control systems subject to uncertain and disturbing conditions. In these, the MOP, which considers different performance requirements, is solved online to obtain different controller configurations at given time intervals to compensate for the undesired behaviors of the controlled system. One example of these tuning methods is found in [22]. In this, the parameters of an inverse dynamics controller for the DC motor are tuned online through different multi-objective variants of DE. The MOP takes into account the system identification error and the parameter sensibility. The adaptively tuned controller achieves a good performance when critical uncertainties are induced to the motor. Nonetheless, there is a lack of studies about adaptive tuning methods based on meta-heuristic optimization, until now it is impossible to determine their effectiveness in controlling complex systems.

B. Contributions

As observed before, there is a lack of studies related to the performance of search approaches (such as the dominance-based, decomposition-based, metric-driven, and hybrid) to find a finite Pareto front approximation (assuming that the true Pareto front is not known in real-world optimization problems) in the adaptive tuning methods based on multi-objective meta-heuristic optimization and subject to hard and uncertain operative conditions; only the dominance-based meta-heuristics have been studied in general for the controller tuning problem as can be observed in [8]. Hence in this paper, the search approaches are studied in the adaptive controller tuning method based on online multi-objective meta-heuristic optimization. A particular case study "a four-bar mechanism" is proposed to implement the adaptive tuning methods based on four different state-of-art meta-heuristic search approaches such as the dominance-based, decomposition-based, metric-driven and hybrid search approaches. Additionally, a novel metric-driven multi-objective variant of the Differential Evolution based on the hypervolume (HV-MODE) is proposed.

The main contributions of this paper are: i) The empirical study of different search approaches in the adaptive tuning methods based on online multi-objective meta-heuristic optimization. ii) The proposal of a multi-objective optimizer which considers a metric-driven search approach and provides improved performance in the adaptive tuning method (online controller tuning problem). iii) The proposal of a MOP for the adaptive controller tuning of dynamic systems, which

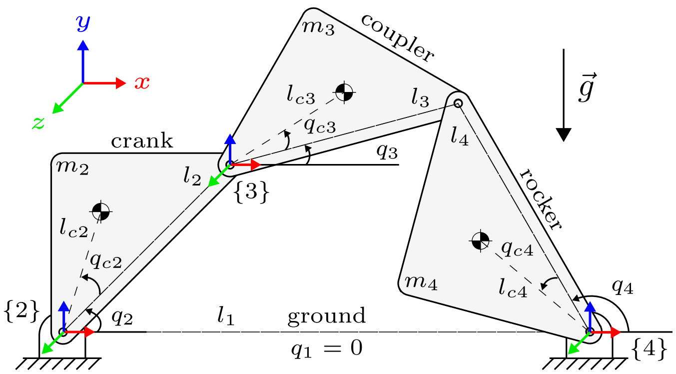

Fig. 1: Generalized four-bar mechanism (GFBM).

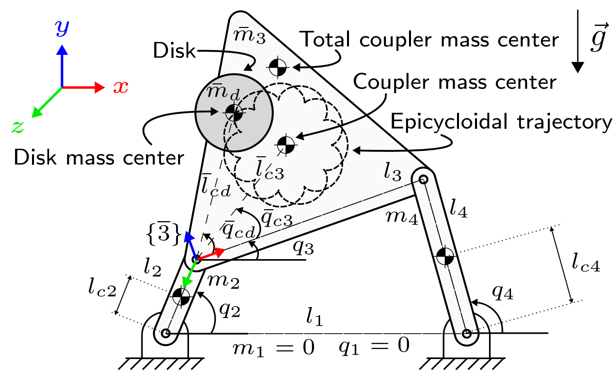

Fig. 2: Real four-bar mechanism (RFBM).

considers the identification error and the smoothness of the control signal. The controller tuning method is applied to the case study of an FBM, where suitable model parameters are obtained online to be used in a PD-computed-torque speed controller.

The rest of the paper is organized as follows: the generalized and the real crank-rocker FBMs are described in Section III. In Section IV, an overview on multi-objective optimization and adaptive controller tuning is given, and then, an adaptive controller tuning strategy based on multi-objective meta-heuristic optimization for the speed control of the FBM is proposed. Four representative state-of-art multi-objective meta-heuristics based on different search approaches are introduced to be used along with the proposed control strategy in Section V. Additionally, the proposed optimizer HV-MODE is described in the same section. Numerical results from the adaptive controller tuning strategies based on the above optimizers in the speed control of a disturbed FBM are presented and discussed in Section VI. Conclusions and future research are given in Section VII.

II. Case study: The four-bar mechanism

Two dynamics are considered in the proposed adaptive controller tuning strategy. The first dynamics, called "generalized four-bar mechanism (GFBM)", represents the generalized behavior of FBMs in a crank-rocker configuration and is used to perform a dynamic simulation in the adaptive mechanism later explained in Section III-D3. The second dynamics, called "real four-bar mechanism (RFBM)", is a particular case of the GFBM and represents the plant to be controlled.

A. The generalized four-bar mechanism

The GFBM (generalized plant) in a crank-rocker configuration is depicted in Fig. 1. In this, l_i is the length, and q_i is the angle of the i-th link concerning the horizontal.

The dynamic parameters of the GFBM ar contained in the vector $\boldsymbol{p}$, where m_i is the mass, I_i is the inertia moment, l_{c_i} is the length to the mass center and q_{c_i} is the angle to the mass center of the i-th link (all regarding the corresponding reference coordinate system $\{i\}$).

$$\boldsymbol{p} = [m_2, m_3, m_4, I_2, I_3, I_4, l_{c_2}, l_{c_3}, l_{c_4}, q_{c_2}, q_{c_3}, q_{c_4}]^T \quad (1)$$

Using the crank position q_2 as the generalized coordinate, the corresponding angles of the rocker and the coupler links can be obtained through a kinematic analysis as:

$$\begin{aligned} q_3 &= 2\tan^{-1}\left(\frac{-k_2 \pm \sqrt{k_1^2+k_2^2-k_3^2}}{k_3-k_1}\right) \\ q_4 &= \tan^{-1}\left(\frac{l_2\sin(q_2)+l_3\sin(q_3)}{-l_1+l_2\cos(q_2)+l_3\cos(q_3)}\right) \end{aligned} \quad (2)$$

where

$$\begin{aligned} k_1 &= 2l_3\left(l_2\cos(q_2) - l_1\right) \\ k_2 &= 2l_2l_3\sin(q_2) \\ k_3 &= l_1^2 + l_2^2 + l_3^2 - l_4^2 - 2l_1l_2\cos(q_2) \end{aligned} \quad (3)$$

Then, the angular velocities of these links can be also expressed regarding q_2, $q_3(q_2)$, $q_4(q_2)$ and the generalized velocity $\dot{q}_2$, as shown in (4).

$$\begin{aligned} \dot{q}_3 &= \frac{l_2}{l_3}\frac{\sin(q_4-q_2)}{\sin(q_3-q_4)}\dot{q}_2 = S_1 \\ \dot{q}_4 &= \frac{l_2}{l_4}\frac{\sin(q_3-q_2)}{\sin(q_3-q_4)}\dot{q}_2 = S_2 \end{aligned} \quad (4)$$

With the above kinematic relationships, it is possible to develop the dynamics of the FBM by substituting the Lagrangian formulation (5) in the Euler-Lagrange equation (7).

$$L = J_1\dot{q}_2^2 + J_2\dot{q}_3^2 + J_3\dot{q}_4^2 + P_1C_1\dot{q}_2\dot{q}_3 + G_1 \quad (5)$$

with

$$\begin{aligned} J_1 &= \tfrac{1}{2}\left(m_2l_{c_2}^2 + I_2 + m_3l_2^2\right) \\ J_2 &= \tfrac{1}{2}\left(m_3l_{c_3}^2 + I_3\right) \\ J_3 &= \tfrac{1}{2}\left(m_4l_{c_4}^2 + I_4\right) \\ P_1 &= m_3l_2l_{c_3} \\ C_1 &= \cos\left(q_2 - q_3 - q_{c_3}\right) \\ G_1 &= -m_2gl_{c_2}\sin\left(q_2 + q_{c_2}\right) - m_3g\left(l_2\sin(q_2)\right. \\ &\quad \left. + l_{c_3}\sin\left(q_3 + q_{c_3}\right)\right) - m_4gl_{c_4}\sin\left(q_4 + q_{c_4}\right) \end{aligned} \quad (6)$$

$$\frac{d}{dt}\left(\frac{\partial L}{\partial \dot{q}_2}\right) - \frac{\partial L}{\partial q_2} = \tau \quad (7)$$

Hence, the equation of motion of this mechanism is given by the following expression:

$$\begin{aligned} &2\left(J_1 + J_2S_1^2 + J_3S_2^2 + P_1C_1S_1\right)\ddot{q}_2 + \left(2J_2S_1D_{S_1}\right. \\ &\left. +2J_3S_2D_{S_2} + P_1S_1D_{C_1} + P_1C_1D_{S_1}\right)\dot{q}_2^2 \\ &-D_{G_1} = \tau \end{aligned} \quad (8)$$

where

$$\begin{aligned} D_{S_1} &= \tfrac{\partial S_1}{\partial q_2} + \tfrac{\partial S_1}{\partial q_3} S_1 + \tfrac{\partial S_1}{\partial q_4} S_2 \\ D_{S_2} &= \tfrac{\partial S_2}{\partial q_2} + \tfrac{\partial S_2}{\partial q_3} S_1 + \tfrac{\partial S_2}{\partial q_4} S_2 \\ D_{C_1} &= \tfrac{\partial C_1}{\partial q_2} + \tfrac{\partial C_1}{\partial q_3} S_1 \\ D_{G_1} &= \tfrac{\partial G_1}{\partial q_2} + \tfrac{\partial G_1}{\partial q_3} S_1 + \tfrac{\partial G_1}{\partial q_4} S_2 \end{aligned} \tag{9}$$

with the derivatives

$$\begin{aligned} \tfrac{\partial S_1}{\partial q_2} &= -\tfrac{l_2}{l_3} \tfrac{\cos(q_2-q_4)}{\sin(q_3-q_4)} \\ \tfrac{\partial S_1}{\partial q_3} &= \tfrac{l_2}{l_3} \tfrac{\sin(q_2-q_4)\cos(q_3-q_4)}{\sin^2(q_3-q_4)} \\ \tfrac{\partial S_1}{\partial q_4} &= -\tfrac{l_2}{l_3} \tfrac{\sin(q_2-q_3)}{\sin^2(q_3-q_4)} \\ \tfrac{\partial S_2}{\partial q_2} &= -\tfrac{l_2}{l_4} \tfrac{\cos(q_2-q_3)}{\sin(q_3-q_4)} \\ \tfrac{\partial S_2}{\partial q_3} &= \tfrac{l_2}{l_4} \tfrac{\sin(q_2-q_4)}{\sin^2(q_3-q_4)} \\ \tfrac{\partial S_2}{\partial q_4} &= -\tfrac{l_2}{l_4} \tfrac{\sin(q_2-q_3)\cos(q_3-q_4)}{\sin^2(q_3-q_4)} \\ \tfrac{\partial C_1}{\partial q_2} &= -\sin(q_2-q_3-q_{c_3}) \\ \tfrac{\partial C_1}{\partial q_3} &= \sin(q_2-q_3-q_{c_3}) \\ \tfrac{\partial G_1}{\partial q_2} &= -m_1 g l_{c_2} \cos(q_2+q_{c_2}) - m_2 g l_2 \cos q_2 \\ \tfrac{\partial G_1}{\partial q_3} &= -m_2 g l_{c_3} \cos(q_3+q_{c_3}) \\ \tfrac{\partial G_1}{\partial q_4} &= -m_3 g l_{c_4} \cos(q_4+q_{c_4}) \end{aligned} \tag{10}$$

The equation of motion in (8) can be arranged in the closed-form (11), where $M(\boldsymbol{p}, q_2)$, $C(\boldsymbol{p}, q_2, \dot{q}_2)$ and $G(\boldsymbol{p}, q_2)$ are the inertia, centrifugal/Coriolis and gravity terms, respectively, and the term τ corresponds to the generalized torque.

$$M(\boldsymbol{p}, q_2)\ddot{q}_2 + C(\boldsymbol{p}, q_2, \dot{q}_2)\dot{q}_2 + G(\boldsymbol{p}, q_2) = \tau \tag{11}$$

Let $\boldsymbol{x} = [x_1, x_2]^T = [q_2, \dot{q}_2]^T$ be the state vector that includes the angular position and speed of the FBM crank. Using (11), the state equation for the closed-loop system can be written as in (12), with $u = \tau$ the control action and t the time.

$$\dot{\boldsymbol{x}} = \begin{bmatrix} x_2 \\ \frac{u - C(\boldsymbol{p}, x_1, x_2)x_2 - G(\boldsymbol{p}, x_1)}{M(\boldsymbol{p}, x_1)} \end{bmatrix} = \boldsymbol{f}(\boldsymbol{p}, \boldsymbol{x}, u, t) \tag{12}$$

The output vector is selected as $\boldsymbol{y} = [y_1, y_2, y_3]^T = [q_2, \dot{q}_2, \ddot{q}_2]^T$ and contains respectively, the position, velocity, and acceleration of the mechanism crank, all of these are assumed to be measurable or observable variables.

B. The real four-bar mechanism

Let the mechanism in Fig. 2 be the RFBM to be controlled (real plant) with the fixed parameters in Table I. This system is a particular case of the GFBM and inherits its kinematics and dynamics. Some important considerations are pointed out next to describe the real mechanism dynamics in the form of (11) and using the same parameter vector as in (1).

1) The real mechanism bars and the disturbing disk: The crank and rocker bars of the RFBM are considered as straight bars, i.e., $q_{c_2} = q_{c_4} = 0$. With the aim of inducing uncertainties, a disk of mass $\bar{m}_d$ and moment of inertia $\bar{I}_d$ is assumed to be rigidly joined to the coupler bar of the real mechanism. The resulting total mass m_3, mass center $\mathbf{c}_3$ and inertia I_3 of the coupler link are described next:

1.1) Total coupler link mass center: The mass and the moment of inertia, both relative to the coupler link without the disk, are denoted by $\bar{m}_3$ and $\bar{I}_3$. Likewise, the relative location of the coupler (without the disk) mass center $\bar{\mathbf{c}}_3$ and the disk mass center $\bar{\mathbf{c}}_d$ in (13) are given by the lengths $\bar{l}_{c_3}$ and $\bar{l}_{c_d}$, and the angles $\bar{q}_{c_3}$ and $\bar{q}_{c_d}$ (all referenced to the coordinate system $\{\bar{3}\}$), respectively.

$$\begin{aligned} \bar{\boldsymbol{c}}_{\boldsymbol{3}} &= \left[\bar{l}_{c_3}\cos(\bar{q}_{c_3}), \bar{l}_{c_3}\sin(\bar{q}_{c_3})\right]^T \\ \bar{\boldsymbol{c}}_{\boldsymbol{d}} &= \left[\bar{l}_{c_d}\cos(\bar{q}_{c_d}), \bar{l}_{c_d}\sin(\bar{q}_{c_d})\right]^T \end{aligned} \tag{13}$$

Then, the total mass center of the coupler link with the disk is represented by the vector $\mathbf{c}_3$ in (14) with the corresponding magnitude l_{c_3} and direction q_{c_3} given by (15) (these also referenced to the coordinate system $\{\bar{3}\}$).

$$\boldsymbol{c}_{\boldsymbol{3}} = \frac{\bar{m}_3\bar{c}_3 + \bar{m}_d\bar{c}_d}{\bar{m}_3 + \bar{m}_d} \tag{14}$$

$$\begin{aligned} l_{c_3} &= \|\boldsymbol{c}_{\boldsymbol{3}}\| \\ q_{c_3} &= \tan^{-1}\left(\frac{\bar{m}_3\bar{l}_{c_3}\sin(\bar{q}_{c_3}) + \bar{m}_d\bar{l}_{c_d}\sin(\bar{q}_{c_d})}{\bar{m}_3\bar{l}_{c_3}\cos(\bar{q}_{c_3}) + \bar{m}_d\bar{l}_{c_d}\cos(\bar{q}_{c_d})}\right) \end{aligned} \tag{15}$$

1.2) Total coupler link mass: The total mass of the coupler with the disk is given by (16).

$$m_3 = \bar{m}_3 + \bar{m}_d \tag{16}$$

1.3) Total coupler link inertia: The total inertia of the coupler with the disk is obtained through the Steiner's theorem in (17).

$$I_3 = \bar{I}_3 + \bar{m}_3\|\boldsymbol{c}_{\boldsymbol{3}} - \bar{\boldsymbol{c}}_{\boldsymbol{3}}\|^2 + \bar{I}_d + \bar{m}_d\|\boldsymbol{c}_{\boldsymbol{3}} - \bar{\boldsymbol{c}}_{\boldsymbol{d}}\|^2 \tag{17}$$

2) The non-linear trajectory of the disk: Additionally, the disk is following a highly non-linear epicycloidal trajectory around the center of mass $\bar{\boldsymbol{c}}_{\boldsymbol{3}}$ as observed in Fig. 2. This trajectory is described by (18) with $r_1 = 60.5 \times 10^{-3}$ and $r_2 = 11 \times 10^{-3}$. Then, the magnitude and the direction to disk mass center vector referenced to the coordinate system $\{\bar{3}\}$ are given by $\bar{l}_{c_d} = \sqrt{\bar{x}_3^2 + \bar{y}_3^2}$ and $\bar{q}_{c_d} = \tan^{-1}(\bar{y}_3/\bar{x}_3)$, respectively. When following the above trajectory, the disk produces non-linear variations in the dynamic parameters of the FBM.

$$\begin{aligned} \bar{x}_3 = \bar{l}_{c_3}\cos(\bar{q}_{c_3}) + (r_1 + r_2)\cos\left(\tfrac{4\pi t}{5}\right) \\ -r_2\cos\left(\tfrac{4\pi t}{5}\left(1 + \tfrac{r_1}{r_2}\right)\right) \\ \bar{y}_3 = \bar{l}_{c_3}\sin(\bar{q}_{c_3}) + (r_1 + r_2)\sin\left(\tfrac{4\pi t}{5}\right) \\ -r_2\sin\left(\tfrac{4\pi t}{5}\left(1 + \tfrac{r_1}{r_2}\right)\right) \end{aligned} \tag{18}$$

III. Adaptive controller tuning based on online multi-objective optimization

An overview of multi-objective optimization, multi-objective meta-heuristics, and adaptive controller tuning is presented in this section. Then, a proposed adaptive controller tuning strategy based on online multi-objective meta-heuristic optimization for the speed regulation of the RFBM in Fig. 2 is described.

TABLE I: Fixed parameters of the real mechanism.

Parameter	Value
l_1	0.3810 (m)
l_2	0.1016 (m)
l_3	0.3048 (m)
l_4	0.2032 (m)
m_2	0.1554 (Kg)
$\bar{m}_3$	3.5110 (Kg)
m_4	0.2996 (Kg)
$\bar{m}_d$	1.1152 (Kg)
I_2	0.0168$\times 10^{-2}$ $(Kg \cdot m^2)$
$\bar{I}_3$	3.2974$\times 10^{-2}$ $(Kg \cdot m^2)$
I_4	0.1137$\times 10^{-2}$ $(Kg \cdot m^2)$
$\bar{I}_d$	0.1394$\times 10^{-2}$ $(Kg \cdot m^2)$
l_{c_2}	0.0508 (m)
$\bar{l}_{c_3}$	0.1759 (m)
l_{c_4}	0.1016 (m)
q_{c_2}	0.0 (rad)
$\bar{q}_{c_3}$	0.5236 (rad)
q_{c_4}	0.0 (rad)
g	9.81 (m/s^2)

A. Multi-objective optimization

A multi-objective optimization problem (MOP) is stated as in (19), where a vector of design variables $\boldsymbol{p} = [p_1, \ldots, p_d]^T$ must be found to minimize a vector $\boldsymbol{F}$ of $m \geq 2$ objective functions which are in conflict with each other. The MOP is subject to several constraints in the form of $g_i(\boldsymbol{p})$ and $h_j(\boldsymbol{p})$, as well as the design variables bounds $p_k \in [p_k^{min}, p_k^{max}]$. The space of feasible solutions (where all constraints are met) is denoted by Ω.

$$\begin{array}{l} \textbf{min } \boldsymbol{F}(\boldsymbol{p}) = [f_1(\boldsymbol{p}), \ldots, f_m(\boldsymbol{p})]^T \\ \text{subject to:} \\ \quad g_i(\boldsymbol{p}) \leq 0, i = 1, \ldots, n_g \\ \quad h_j(\boldsymbol{p}) = 0, j = 1, \ldots, n_h \\ p_k^{min} \leq p_k \leq p_k^{max}, k = 1, \ldots, d \end{array} \tag{19}$$

Definition 1. *(Pareto dominance, [23]).*
A vector $\boldsymbol{F}(\boldsymbol{p}) = [f_1(\boldsymbol{p}), \ldots, f_m(\boldsymbol{p})]^T$ is said to dominate $\boldsymbol{F}(\boldsymbol{q}) = [f_1(\boldsymbol{q}), \ldots, f_m(\boldsymbol{q})]^T$ (denoted by $\boldsymbol{F}(\boldsymbol{p}) \preceq \boldsymbol{F}(\boldsymbol{q})$) if and only if $\boldsymbol{F}(\boldsymbol{p})$ is as good as $\boldsymbol{F}(\boldsymbol{q})$ for all the objectives, i.e., $f_i(\boldsymbol{p}) \leq f_i(\boldsymbol{q}), \forall i \in \{1, \ldots, m\}$, and for at least one objective $f_i(\boldsymbol{p}) < f_i(\boldsymbol{q})$.

Definition 2. *(Pareto optimality, [23]).*
A decision vector $\boldsymbol{p} \in \Omega$ is a Pareto optimal if no objective function $f_i(\boldsymbol{p})$ can be improved without worsening the rest, i.e., $\nexists \boldsymbol{q} \in \Omega$ such that $\boldsymbol{F}(\boldsymbol{q}) \preceq \boldsymbol{F}(\boldsymbol{p})$.

Definition 3. *(Pareto optimal set, [23]).*
The Pareto optimal set $\mathcal{P}^*$ contains every possible optimal decision vector $\boldsymbol{p} \in \Omega$, i.e., $\mathcal{P}^* = \{\boldsymbol{p} \in \Omega \mid \nexists \boldsymbol{q} \in \Omega,\ \boldsymbol{q} \preceq \boldsymbol{p}\}$.

Definition 4. *(Pareto front, [23]).*
The Pareto front also named true Pareto front contains the evaluated objective vectors of the vectors in $\mathcal{P}^*$, i.e., $\mathcal{PF}^* = \{\boldsymbol{F}(\boldsymbol{p}) \mid \boldsymbol{p} \in \mathcal{P}^*\}$.

The solution of the MOP in (19) is a set of Pareto optimal solutions $\mathcal{P}^*$, that mapped in the objective function space, provide a set $\mathcal{PF}^*$ with different trade-offs among objectives. Then, the decision maker can select a suitable trade-off solution for a particular application depending on its preferences.

B. Multi-objective meta-heuristics

Meta-heuristic optimizers are stochastic computational techniques that can find good solutions to optimization problems, at a reasonable computational cost. Many of them are inspired in several biological processes such as the natural evolution. Among the advantages of these techniques is their capability to solve very complex problems (e.g., with highly non-linear or discontinuous elements) without requiring additional information about them (e.g., derivatives).

A multi-objective meta-heuristic optimizer can solve MOPs and find several trade-offs among objectives. These trade-offs conform a finite Pareto front approximation $\mathcal{PF}^A$ to the true Pareto front $\mathcal{PF}^*$. The search for this approximation can be performed based on the following four approaches [24], [25]:

1) Dominance-based: the Pareto dominance is used to identify promising candidate solutions, i.e., solutions that are non-dominated are preferred and must persist.
2) Decomposition-based: the MOP is decomposed into a finite number of scalar optimization sub-problems which are optimized simultaneously as single-objective problems.
3) Metric-driven: a performance metric which evaluates the quality of each solution (concerning a candidate solution set or a reference alternative) is used to decide which solutions are better to guide the search.
4) Hybrid: in this, the above search approaches are adopted.

Despite the adopted search approach, meta-heuristics must be able to find a suitable $\mathcal{PF}^A$ with high-quality trade-offs according to several desirable features measurable with different indicators [26]:

1) Capacity: is related to the number of different trade-offs in $\mathcal{PF}^A$. A large number of alternatives is preferred.
2) Convergence: is the closeness of $\mathcal{PF}^A$ to $\mathcal{PF}^*$.
3) Diversity: is the degree of similarity among trade-offs in $\mathcal{PF}^A$. Since $\mathcal{PF}^A$ contains a finite number of trade-offs, less similar solutions are preferred.
4) Pertinence: is the closeness of solutions in $\mathcal{PF}^A$ to preferred trade-offs or regions of objective functions space (these are commonly established *a priori*).

C. General adaptive control strategy

One of the requirements to establish the proper controller parameters is to know the dynamic model of the plant to be controlled [27]. When the plant is subject to unknown and large uncertainties or disturbances, its dynamic model varies, and the controller parameters must be updated recurrently to maintain the desired control performance.

Fig. 3 shows the general adaptive control scheme detailed in [27]. In this, the generalized dynamic model of the real plant is estimated online by using its inputs and outputs, i.e., its injected control signals and measured responses. By using this generalized dynamic model, the controller parameters can be properly adjusted to fulfill a set of well-established performance specifications.

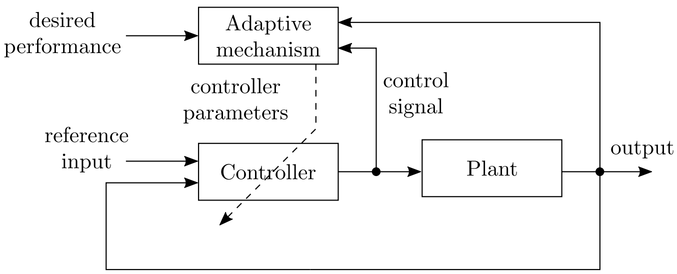

Fig. 3: General adaptive control scheme.

D. Proposed adaptive controller tuning strategy based on online multi-objective meta-heuristic optimization

Fig. 4 shows the proposed adaptive control strategy for the speed regulation of the FBM. In this, the real mechanism, which can be subject to uncertainties or disturbances, is handled by a model based controller whose parameters are in turn adjusted by an adaptive mechanism. The adaptive mechanism uses information about the real plant outputs and control signals to estimate its generalized model parameters. This estimation is performed through an online multi-objective meta-heuristic optimization approach. In this, a MOP is stated by considering several conflicting performance criteria and constraints about the possible parameter configurations. The performance of a given parameter configuration is measured by performing first a dynamic simulation within a short backward time window. The MOP is then solved by a multi-objective meta-heuristic optimizer to obtain a set of feasible solutions with different performance trade-offs. Finally, the decision maker selects a single best trade-off solution among the obtained alternatives using preferences; this solution contains a suitable set of model parameters that are later implanted in the model-based controller. This adaptation is performed for each sampling instant during the execution of the speed regulation task of the real mechanism.

The elements of the proposed adaptive control strategy are described in detail below.

1) Real plant: The RFBM obeys the state equation $\dot{\boldsymbol{x}} = \boldsymbol{f}(\boldsymbol{p}, \boldsymbol{x}, u, t)$ in (12) and includes the dynamic parameters $\boldsymbol{p}$ in (1) described in Section II-B. The output vector of this mechanism is denoted by $\mathbf{y}$ and includes the measurable and observable variables given in Section II-A, i.e., the angular position, speed and acceleration of the real mechanism crank.

2) Controller: In order to regulate the speed of the RFBM crank to a desired speed profile $\boldsymbol{y_d} = [\dot{q}_d, \ddot{q}_d]^T = [\dot{q}_d, 0]^T$, where $\dot{q}_d$ and $\ddot{q}_d$ are the desired crank speed and acceleration, a PD-computed-torque controller is adopted.

Computed-torque controllers are effective alternatives to control robotic manipulators [28]. Nevertheless, the main drawback with these controllers is that require an accurate dynamic model of the plant to operate properly, i.e., all the physical parameters, as well as the uncertainties and disturbances must be known and modeled in a precise way. If an accurate model is provided, it is possible to ensure globally asymptotic stability with a computed-torque controller. In the opposite case, the performance of the controller is diminished in proportion to the inconsistencies between the real plant and the provided model.

To overcome the above difficulty, the parameters of the controller are updated by the adaptive mechanism based on the meta-heuristic multi-objective optimization approach, which online finds an accurate GFBM dynamic model equivalent to the one of the RFBM, valid in a backward time window $w\triangle t$ where the inputs and outputs of the real plant are used for the estimation, with $\triangle t$ the sampling time interval and $w \in \mathbb{Z}^+$ the number of backward sampling instants. The adopted PD-computed-torque controller is described by (20), where $v = K_p e + K_d \dot{e}$, $e = y_{d,1} - y_2$ and $\dot{e} = y_{d,2} - y_3$, with $K_p = 70$ and $K_d = 0.01$ the proportional and derivative gains. The vector $\hat{\boldsymbol{p}}^*$ contains the most suitable GFBM dynamic parameters (1) that match the RFBM behavior.

$$\begin{aligned} u &= M(\hat{\boldsymbol{p}}^*, q_2)v + C(\hat{\boldsymbol{p}}^*, q_2, \dot{q}_2)\dot{q}_2 + G(\hat{\boldsymbol{p}}^*, q_2) \\ &= f_u(\hat{\boldsymbol{p}}^*, \boldsymbol{y}, \boldsymbol{y_d}, t) \end{aligned} \tag{20}$$

It is important to mention that when $t < w\triangle t$, there is not enough past information about the real plant inputs and outputs, then the adaptation is not performed and an open-loop constant control signal u_0 must be adopted.

3) Dynamic simulation: In order to select the most suitable parameter configuration $\hat{\boldsymbol{p}}^*$, the performance of different alternatives $\hat{\boldsymbol{p}}$ must be measured by performing first a dynamic simulation. For this, the generalized plant is governed by the state equation $\dot{\hat{\boldsymbol{x}}} = \boldsymbol{f}(\hat{\boldsymbol{p}}, \hat{\boldsymbol{x}}, u, \hat{t})$ in (12) and includes the dynamic parameters $\hat{\boldsymbol{p}}$ (this encompasses the dynamic parameters given in (1)). The generalized plant output vector $\hat{\boldsymbol{y}}$ has the measurable and observable variables given in Section II-A, i.e., the angular position, speed and acceleration of the generalized mechanism crank.

This dynamic simulation is done under the following conditions:

- The simulation is performed in the time interval $\hat{t} \in [0, w\triangle t]$ using the past information (outputs and control signals) acquired from the real control system within the time window $t \in [t_a - w\triangle t, t_a]$, where t_a is the time instant when the adaptation is performed (i.e., when the adaptive mechanism is invoked).
- The initial conditions of the state equation $\dot{\hat{\boldsymbol{x}}} = \boldsymbol{f}(\hat{\boldsymbol{p}}, \hat{\boldsymbol{x}}, u, \hat{t})$ are $\hat{x}_1(\hat{t} = 0) = y_1(t = t_a - w\triangle t)$ and $\hat{x}_2(\hat{t} = 0) = y_2(t = t_a - w\triangle t)$.
- The control action applied for each simulated time instant is $\hat{u}(\hat{t} = i\triangle\hat{t}) = u(t = t_a - (w-i)\triangle t), i = 0, \ldots, w-1$.

By taking into account the above conditions, the state equation $\dot{\hat{\boldsymbol{x}}} = \boldsymbol{f}(\hat{\boldsymbol{p}}, \hat{\boldsymbol{x}}, u, \hat{t})$ can be solved with a numerical integration method for each simulated sampling instant $\triangle\hat{t}$ and a set of simulated outputs $\hat{\boldsymbol{y}}(\hat{t})$ can be obtained for the whole simulated time interval.

4) Multi-objective optimization problem: Two performance specifications are considered to evaluate a given parameter configuration $\hat{\boldsymbol{p}}$: the degree of similarity between the real plant and the generalized plant regarding their outputs within a short backward time window (starting with the same initial conditions and using the same control signals), and the smoothness of the computed control signal.

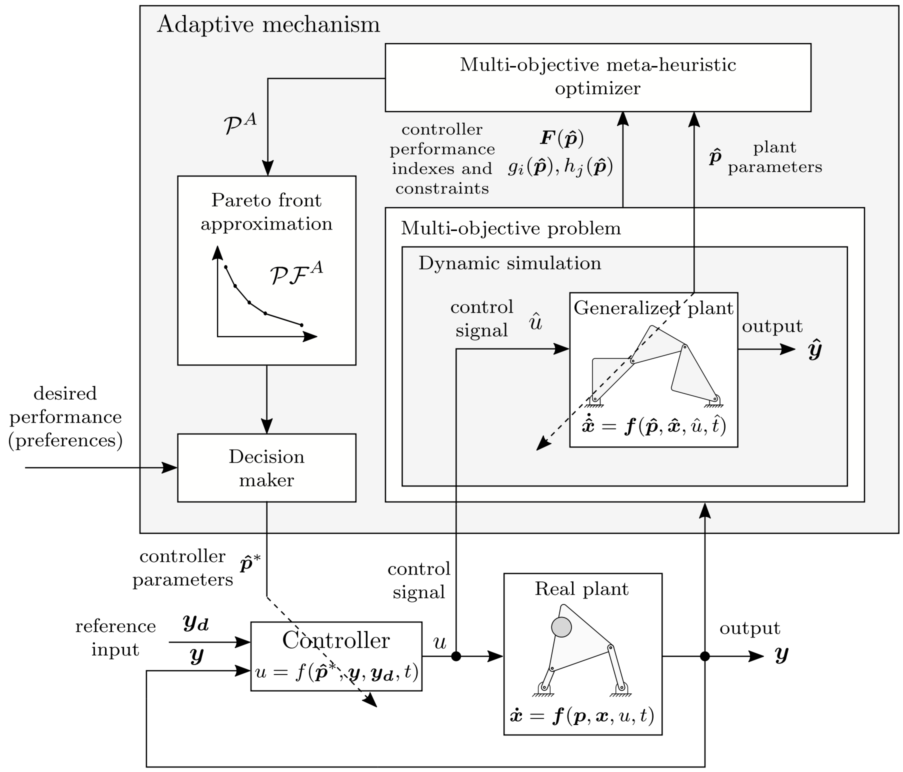

Fig. 4: Proposed adaptive controller tuning strategy based on online multi-objective meta-heuristic optimization.

The first criterion implies that the vector of parameters $\hat{\boldsymbol{p}}$ must minimize the differences between the real and generalized mechanisms within the time window $t \in [t_a - w\triangle t, t_a]$ regarding their outputs $\boldsymbol{y}$ and $\hat{\boldsymbol{y}}$, respectively. This degree of similarity is measured with the integral squared error (ISE) performance index as observed in (21). Then, with the best parameter configuration $\hat{\boldsymbol{p}}^*$, the dynamics of the generalized mechanism is equivalent to this of the real one for the mentioned time window and $\hat{\boldsymbol{p}}^*$ is suitable to be used in the PD-computed-torque controller. A higher degree of similarity between the outputs $\boldsymbol{y}$ and $\hat{\boldsymbol{y}}$ implies a better estimation of the real plant behavior, which leads to an accurate speed regulation when the generalized plant parameters are used in the PD-computed-torque controller.

$$f_1(\hat{\boldsymbol{p}}) = \int_{T=t_a-w\triangle t}^{t_a} \left(\boldsymbol{y}(T) - \hat{\boldsymbol{y}}(T - t_a + w\triangle t)\right)^2 dT \quad (21)$$

With the second specification, the parameter vector $\hat{\boldsymbol{p}}$ must minimize the difference between the control signals computed in the adaptation time instant $u(t_a)$ and calculated for the previous adaptation instant $u(t_a - \triangle t)$. The smoothness of the control signal is then measured with the squared difference in (22). With a suitable $\hat{\boldsymbol{p}}^*$, the variations of the control signal are diminished. If the control signal is smooth enough, the wear of the real mechanism is reduced.

$$f_2(\hat{\boldsymbol{p}}) = \left(u(t_a) - u(t_a - \triangle t)\right)^2 \quad (22)$$

As it can be noticed, there is a trade-off between these criteria; since the real mechanism has a highly non-linear behavior, an excessively smooth control action (e.g., with a constant or linear behavior) cannot provide a suitable speed accuracy.

The conflicting specifications in (21) and (22) can be considered as the objectives of the MOP in (23) which is subject to the initial conditions and to the limits of the actuation device u_{min} and u_{max} (regarding the applied torque). Additionally, the problem is implicitly constrained by the dynamic behaviors of the real and generalized mechanisms, described by $\dot{\boldsymbol{x}} = \boldsymbol{f}(\boldsymbol{p}, \boldsymbol{x}, u, t)$ and $\dot{\hat{\boldsymbol{x}}} = \boldsymbol{f}(\hat{\boldsymbol{p}}, \hat{\boldsymbol{x}}, u, \hat{t})$, respectively. The bounds of the design variables are shown in Table II.

$$\begin{aligned} &\textbf{min } \boldsymbol{F}(\hat{\boldsymbol{p}}) = [f_1(\hat{\boldsymbol{p}}), f_2(\hat{\boldsymbol{p}})]^T \\ &\text{subject to:} \\ &\quad u(t_a + \triangle t) - u_{max} \leq 0 \\ &\quad u_{min} - u(t_a + \triangle t) \leq 0 \\ &\quad \hat{x}_1(0) - y_1(t_a - w\triangle t) = 0 \\ &\quad \hat{x}_2(0) - y_2(t_a - w\triangle t) = 0 \\ &\hat{p}_k^{min} \leq \hat{p}_k \leq \hat{p}_k^{max}, k = 1, \ldots, 12 \end{aligned} \quad (23)$$

5) Multi-objective meta-heuristic optimizer: The MOP in (23) has highly non-linear objectives and constraints. Moreover, it must be solved online to provide a suitable controller adaptation to the changes of the real mechanism for each sampling instant $\triangle t$. Then, this problem is a suitable candidate to be solved by using meta-heuristics.

It is necessary to compare a reasonable number of alternatives using different metrics to evaluate their performance as established in the "No Free Lunch" and "Free Leftovers" theorems [29] to opt for a single multi-objective optimizer in the adaptive controller tuning problem.

TABLE II: Design variables bounds

Variable ($\hat{p}_k$)	Lower bound ($\hat{p}_k^{min}$)	Upper bound ($\hat{p}_k^{max}$)
$\hat{p}_1$ ($\hat{m}_2$)	0.0 (Kg)	3.0 (Kg)
$\hat{p}_2$ ($\hat{m}_3$)	0.0 (Kg)	3.0 (Kg)
$\hat{p}_3$ ($\hat{m}_4$)	0.0 (Kg)	3.0 (Kg)
$\hat{p}_4$ ($\hat{I}_2$)	0.0 ($Kg \cdot m^2$)	0.1604 $\times 10^{-2}$ ($Kg \cdot m^2$)
$\hat{p}_5$ ($\hat{I}_3$)	0.0 ($Kg \cdot m^2$)	0.3261 ($Kg \cdot m^2$)
$\hat{p}_6$ ($\hat{I}_4$)	0.0 ($Kg \cdot m^2$)	1.2370 $\times 10^{-2}$ ($Kg \cdot m^2$)
$\hat{p}_7$ ($\hat{l}_{c_2}$)	0.0 (m)	0.1016 (m)
$\hat{p}_8$ ($\hat{l}_{c_3}$)	0.0 (m)	0.3048 (m)
$\hat{p}_9$ ($\hat{l}_{c_4}$)	0.0 (m)	0.2032 (m)
$\hat{p}_{10}$ ($\hat{q}_{c_2}$)	0.0 (rad)	0.7854 (rad)
$\hat{p}_{11}$ ($\hat{q}_{c_3}$)	0.0 (rad)	0.7854 (rad)
$\hat{p}_{12}$ ($\hat{q}_{c_4}$)	0.0 (rad)	0.7854 (rad)

Because of this, four state-of-art multi-objective meta-heuristic optimizers based on different search approaches (dominance-based, decomposition-based, metric-driven and hybrid) and a proposed metric-driven variant of DE, are selected to analyze the performance of the adaptive tuning mechanism and then identify the most promising alternatives for the adaptive controller tuning problem. Such search approaches are included in the following algorithms: NSGA-II, MOEA/D-DE, SMS-EMOA, NSGA-III and HV-MODE. The above optimizers are described in Section IV.

6) Pareto front approximation: Each time (i.e., for each sampling instant $\triangle t$) that the MOP in (23) is solved by one of the selected optimizers, a different Pareto set approximation $\mathcal{P}^A$, mapped in the objective functions space as the $\mathcal{PF}^A$, is obtained. The $\mathcal{PF}^A$ includes several trade-offs between the objectives previously described.

7) Decision maker: According to a set of preferences, the decision maker can choose a solution in the $\mathcal{PF}^A$ and implant it in the controller. These preferences can be handled in three different ways [23]: *a priori*, *a posteriori* and progressively.

In the *a priori* preference handling, decision making is performed before the search, i.e., a set of well-established preferences is required to exclude less interesting areas from the search. Since the adaptive control system is supposed to involve unknown uncertainties and disturbances, these preferences cannot be described *a priori*. On the other hand, *a posteriori* preference handling methods are responsible for selecting the best trade-off once that the $\mathcal{PF}^A$ is obtained. Progressive methods by their part, alter the preferences during the search for the $\mathcal{PF}^A$ by incorporating the acquired knowledge about this. Both approaches are suitable to be used in adaptive control, but *a posteriori* ones require less computational effort.

Preference handling methods can also be grouped according to the type of the used decision maker; this can be a human designer or an automated entity. Human designers base their decisions on empirical and qualitative observations of the $\mathcal{PF}^A$, while the automated ones use quantitative information of the $\mathcal{PF}^A$ to select the best trade-off.

Since different $\mathcal{PF}^A$s are obtained online (in short intervals of $\triangle t$), the use of a human designer is not possible.

For these reasons, an automated decision maker which handles preferences *a posteriori* is adopted in this work. For this, the knee trade-off of the $\mathcal{PF}^A$ is selected as the best alternative for each sampling time instant $\triangle t$ and is implanted in the controller.

IV. Multi-objective meta-heuristic optimizers

The operation of different search approaches into the optimizers selected to work along with the adaptive mechanism in the proposed adaptive control strategy is presented in this section.

A. Dominance-based

NSGA-II: The non-dominated sorting genetic algorithm II (NSGA-II) is a widely used multi-objective optimizer due its simplicity and effectiveness in solving a variety of constrained MOPs [10]. The fitness of solutions in population is determined by the non-dominated sorting (NDS) where the feasibility, non-domination level and crowding of each solution are taken into account. Better solutions have more chances to generate offsprings through crossover and mutation operations. The size of the entire population that includes parents and offsprings is pruned to preserve only a fixed number of the fittest solutions for each generation.

B. Decomposition-based

MOEA/D-DE: The Multi-objective Evolutionary Algorithm based on Decomposition and Differential Evolution (MOEA-D/DE) is a well-known optimizer in which the MOP is decomposed in several scalar sub-problems which are optimized simultaneously [30]. Together, solutions of all sub-problems conform a Pareto front approximation. Each solution in population is associated to a sub-problem. Sub-problems are grouped into neighborhoods, and their corresponding individuals are recombined and mutated to exploit better alternatives.

C. Metric-driven

SMS-EMOA: The S-Metric Selection Evolutionary Multi-objective Algorithm (SMS-EMOA) is a metric-driven optimizer that uses the hypervolume to guide the search for the Pareto front approximation [25]. As in NSGA-II, the population is ranked by using the NDS. For each generation, a single offspring is generated from the population. The population size is maintained fixed by discarding the worst solution (according to the NDS fitness). If all solutions have the same non-domination level, the hypervolume metric is used to determine the contribution of each solution to the Pareto front, and the alternative that contributes the least is discarded.

Proposed HV-MODE: Differential Evolution (DE) is a meta-heuristic optimizer originally designed for global optimization that bases its operation in the process of natural evolution [31]. This optimizer uses three evolutionary operations in searching for solutions: mutation, crossover, and selection.

In this work, a hypervolume based multi-objective differential evolution (HV-MODE) is proposed. This variant operation is shown in Algorithm 1.

In HV-MODE, an initial population $\boldsymbol{X}$ with NP individuals is generated in the search space. An external archive $\boldsymbol{X}^{ext}$ is adopted in this variant to store all the non-dominated solutions obtained during the evolutionary process.

Algorithm 1: Hypervolume based Multi-objective Differential Evolution (HV-MODE)

Generate initial population $\boldsymbol{X}$ with NP individuals.
Evaluate individuals in $\boldsymbol{X}$.
$\boldsymbol{X}^{ext} \leftarrow \emptyset$
$G \leftarrow 0$
while $G < G_{max}$ **do**
    Update $\boldsymbol{X}^{ext}$.
    foreach $\boldsymbol{x}_k^{ext} \in \boldsymbol{X}^{ext}$ **do**
        $P_k \leftarrow HV\left(\boldsymbol{X}^{ext}, \boldsymbol{0}\right) - HV\left(\boldsymbol{X}^{ext} - \left\{\boldsymbol{x}_k^{ext}\right\}, \boldsymbol{0}\right)$.
    Sort individuals in $\boldsymbol{X}^{ext}$ (using P_i in ascending order).
    foreach $\boldsymbol{x}_i \in \boldsymbol{X}$ **do**
        if $PC \cdot [\boldsymbol{X}^{ext}] < 1$ **then**
            Generate a mutant individual $\boldsymbol{v}_i$ (using (26)).
        else
            Generate a mutant individual $\boldsymbol{v}_i$ (using (25)).
        Generate an offspring individual $\boldsymbol{u}_i$ (using (27)).
        Evaluate $\boldsymbol{u}_i$.
    Select individuals for G+1.
    $G \leftarrow G + 1$

All solutions in $\boldsymbol{X}^{ext}$ are sorted according to their contribution to the archived Pareto front. The hypervolume (HV) metric defined in (24) is used to measure this contribution, where $\boldsymbol{S}$ is a set of non-dominated solutions, $\boldsymbol{r}$ is a reference point and v_k is the hypervolume between the k-th solution in $\boldsymbol{S}$ (mapped in the objective functions space) and $\boldsymbol{r}$. This metric helps to determine the convergence degree of $\boldsymbol{S}$ and the diversity of its solutions [26]. If the origin is selected as the reference point $\boldsymbol{r}$, a lower value of HV implies a better quality of $\boldsymbol{S}$. The contribution of a solution $\boldsymbol{x}_k^v$ is then given by $P_k = HV\left(\boldsymbol{X}^v, \boldsymbol{0}\right) - HV\left(\boldsymbol{X}^v - \left\{\boldsymbol{x}_k^v\right\}, \boldsymbol{0}\right)$.

$$HV\left(\boldsymbol{S}, \boldsymbol{r}\right) = \bigcup_{k=1}^{[\boldsymbol{S}]} v_k \tag{24}$$

During G_{max} generations, individuals in population are mutated and recombined to generate new alternatives. If there is enough information in $\boldsymbol{X}^{ext}$ according to $PC \cdot [\boldsymbol{X}^{ext}] \geq 1$, with PC a percentage of the solutions in the external archive, then each solution $\boldsymbol{x}_i$ in population generates a mutant vector $\boldsymbol{v}_i$ with (25) as in the variant "DE/current-to-pbest/1" in [32]. In this, the $pbest$ solution is randomly selected from the most PC valuable solutions in $\boldsymbol{X}^{ext}$ (according to P_k) while the solutions $\boldsymbol{x}_{r_1}$ and $\boldsymbol{x}_{r_2}$ are two randomly selected individuals such that $r_1 \neq r_2 \neq i$, and F, K are the mutation rates. The above allows to perform an exploitation of individuals when enough potential search regions, lead by solutions in $\boldsymbol{X}^{ext}$, are identified.

$$\boldsymbol{v}_i = \boldsymbol{x}_i + F \cdot (\boldsymbol{x}_{pbest}^{ext} - \boldsymbol{x}_i) + K \cdot (\boldsymbol{x}_{r_2} - \boldsymbol{x}_{r_3}) \tag{25}$$

In the opposite case when $PC \cdot \left[\boldsymbol{X}^{ext}\right] < 1$, this mutant vector $\boldsymbol{v}_i$ is generated by (26) using solutions in population as in the variant "DE/current-to-rand" [33]. In this case, $\boldsymbol{x}_{r_1}$, $\boldsymbol{x}_{r_2}$ and $\boldsymbol{x}_{r_3}$ are three randomly selected individuals such that $r_1 \neq r_2 \neq r_3 \neq i$, and F, K are the mutation rates. This mutation approach enhances the exploratory search when not enough potential search regions are identified.

$$\boldsymbol{v}_i = \boldsymbol{x}_i + F \cdot (\boldsymbol{x}_{r_1} - \boldsymbol{x}_i) + K \cdot (\boldsymbol{x}_{r_2} - \boldsymbol{x}_{r_3}) \tag{26}$$

Once the mutant individual $\boldsymbol{v}_i$ is generated, it can be recombined with $\boldsymbol{x}_i$ to obtain an offspring $\boldsymbol{u}_i$ by using the binomial crossover in (27) for each design variable j with CR the crossover rate and j_{rand} a randomly selected design variable.

$$\boldsymbol{u}_{i,j} = \begin{cases} \boldsymbol{v}_{i,j}, & \textbf{if } rand(0,1) \leq CR \textbf{ or } j = j_{rand} \\ \boldsymbol{x}_{i,j}, & \textbf{otherwise} \end{cases} \tag{27}$$

At the end of each generation, the Pareto dominance generalization of the tournament selection operator in [34] is used to decide among the individuals in the population and their offsprings, the alternatives that are preserved for the next generation based on dominance and feasibility.

When the last generation is reached, the best trade-off solutions are found in the external archive.

D. Hybrid

NSGA-III: The Non-dominated Sorting Genetic Algorithm III (NSGA-III) is a recent optimizer based on NSGA-II which includes a reference-point based selection mechanism that promotes solutions close to a set of preferred points [35], [36]. As in NSGA-II, the population is ranked by using the NDS. For each generation, individuals in the population are recombined to generate offsprings which can be mutated. Individuals that persist in the population are those with the best level of non-domination. If the population size is exceeded, some solutions with the last accepted level of non-domination are removed by using niching concerning a normalized hyper-plane with different reference solutions in the objective function space. For this, solutions in population must also be normalized. This process takes into account some decomposition-approach ideas to establish the proper normalization ranges of each objective.

V. Tests and results

A. Test design

For test in simulation, the crank speed of the RFBM in Fig. 2 must be regulated to $\dot{q}_d = 2\pi$ (rad/s) during 5 (s).

The sampling time instant is chosen as $\triangle t = 5$ (ms) and the number of backward sampling instants as $w = 10$. The gains of the PD-computed-torque controller are empirically set as $K_p = 70$ and $K_d = 0.01$. The limits of the actuation device are selected as $u_{min} = -7$ $(N \cdot m)$ and $u_{max} = 7$ $(N \cdot m)$. Finally, the initial control signal (applied when $t \in [0, w\triangle t]$) is $u_0 = 6$ $(N \cdot m)$.

The optimizers NSGA-II, MOEA/D-DE, SMS-EMOA, NSGA-III, and HV-MODE, which use different search approaches, are used in the adaptive mechanism of the tuning strategy; then, the strategies based on these are referred with the name of the optimizer prefixed by "ACTS-" (from adaptive controller tuning strategy).

In this work, the SBX crossover and the Polynomial mutation operators are used in NSGA-II, SMS-EMOA, and

TABLE III: Parameters of the multi-objective meta-heuristic optimizers

Optimizer	Parameters		
NSGA-II	$pm = 0.083$	$pc = 0.9$	$\eta_c = 20$
	$\eta_m = 100$		
MOEA/D-DE	$F = 0.5$	$CR = 0.5$	$T = 6$
SMS-EMOA	$pm = 0.083$	$pc = 1.0$	$\eta_c = 20$
	$\eta_m = 100$		
NSGA-III	$pm = 0.083$	$pc = 0.9$	$\eta_c = 20$
	$\eta_m = 100$	$p = 4$	
HV-MODE	$F = 0.5$	$K = 0.5$	$CR = 0.5$
	$PC = 0.25$		

NSGA-III, as in the original versions of these optimizers. For MOEA/D-DE, the Tchebycheff decomposition approach and the evolutionary operators of the "DE/rand/1/bin" variant of differential evolution [37] are adopted because of its recurrently use and proven high performance in multi-objective optimization [38].

The parameters of these meta-heuristics are shown in Table III. The population size for all alternatives is set as $NP = 30$, and the maximum number of generations as $G_{max} = 120$ except for SMS-EMOA, i.e., 3600 evaluations of the objective function vector are performed per optimization process. In SMS-EMOA, the population size is chosen as $NP = 30$ and $G_{max} = 3600$ iterations are performed since only one offspring is generated and evaluated per generation. The above parameters are selected by trial and error, starting from the configurations suggested on their original papers, and slightly increasing/decreasing them until no improvement is obtained regarding the mean hypervolume in the ACTS execution.

B. Analysis of results

A single execution of all control alternatives based on five optimizers from different search approaches is analyzed. Since for each single execution of a control alternative, the control parameters must be adapted in every sampling instant $\triangle t$ (starting from $(w + 1)\triangle t$) during 5 (s), a total of 989 optimization processes are performed, and the same number of Pareto front approximations are obtained.

Table IV shows the speed regulation performance of each control alternative concerning the integral absolute error (IAE), the integral time-weighted absolute error (ITAE), the integral squared error (ISE) and the integral time-weighted squared error (ITSE) [39]. The control signal smoothness is measured by the integral of the absolute value of the derivative control signal (IADU) [40]. The above measurements are calculated when all alternatives reach the reference signal, i.e., in the time interval $t \in [0.5, 5]$ (s) for both scenarios.

In Table IV, different trade-offs between the speed regulation performance (regarding IAE, ITAE, ISE, and ITSE) and the smoothness of the control signal (IADU) can be observed. Two alternatives stand out from others since they achieve the best performances according to the control measurements, these are ACTS-SMS-EMOA and ACTS-HV-MODE whose optimizers are from the metric-driven search approach. With ACTS-SMS-EMOA, the lowest regulation error is achieved while the smoothest control signal is obtained with ACTS-HV-MODE.

It is important to remark that the above performance trade-offs are obtained by selecting the knee solution from every found Pareto front approximation, no matter the selected optimizer. If the application requires it, a different trade-off solution can be chosen by using a different preference handling method [40] to balance the objectives or prioritize one of them more than the other.

As a matter of reference, Table IV shows the performance of a PI controller (with $K_p = 6.778$ and $K_i = 0.097$ the iteratively tuned proportional and integral gains, respectively), a widely used controller in the industry for speed regulation [41]. It is observed that the speed regulation error of the PI controller (regarding IAE, ITAE, ISE and ITSE indicators) is more than 1300% of the regulation error achieved with ACTS-HV-MODE. Concerning the smoothness of the control signal, the IADU value of the PI controller is between the 90% and 97% of the proposed strategies, which is due to the PI controller linear behavior.

The behavior of all adaptive controller tuning strategies can be observed in Fig. 5. The left column shows the crank speed and its error (concerning the reference signal) achieved with all alternatives. In the right column are the applied control signal and its variations for all strategies. The different trade-offs between the speed regulation performance and the control action smoothness are observed in the sub-plots.

Additionally, the performance of the search approaches adopted by the selected optimizers is analyzed during the execution of its corresponding adaptive control strategy. For this, the quality of each Pareto front approximation (from the 989 fronts obtained in a single execution) is evaluated by using the hypervolume indicator in (24) using the origin as the reference point, and the two-set-coverage metric. The two-set-coverage metric (also named C-metric) determines the overlaps between two different Pareto front approximations regarding the ratio of non-dominated solutions.

Table V shows the mean and standard deviation values of the calculated hypervolumes. In this, the metric-driven and hybrid optimizers have the best values of hypervolume. It is also observed that the HV-MODE from the metric-driven search approach finds the best Pareto front approximations regarding diversity and convergence.

In addition to the descriptive statistical results, the Wilcoxon test is performed by pairs of the hypervolume samples obtained with each optimizer to determine if the differences between results are significant and are not due to chance. For this, the "two-sided" alternative hypothesis is selected, which establishes that medians of two different samples are significantly different, i.e., one alternative performs better than the other. On the other hand, the "null" hypothesis establishes the opposite, i.e., the medians are close, and no significant differences are found.

The results of the Wilcoxon test for the hypervolume samples are shown in Table VI. In this, the R_+ column indicates the times that the first alternative overcomes the second one and the R_- column denotes the opposite. The column $p\text{-}value$ shows the probability of accepting the null hypothesis, then values below 0.05 (by setting the statistical significance as 5%) allow valid conclusions to be drawn. The winner alternatives are highlighted in boldface. According to these results, the metric-driven and hybrid optimizers show to have an outstanding performance since they can find diverse and convergent Pareto front approximations. In the same way, HV-MODE turned out to be the most promising optimizer, since the hypervolumes of its obtained approximations are significantly better than the ones from the other alternatives. Another good performing alternative is NSGA-III which is followed by NSGA-II, SMS-EMOA, and MOEA/D-DE regarding the number of wins.

The obtained results concerning the C-metric are shown in Table VII. In this, the C-metric is computed over the approximations obtained for each time instant with a pair of optimizers. The winner of each pairwise comparison is shown in boldface. According to the number of wins, the metric-driven optimizers has the best coverage of non-dominated solutions. The HV-MODE turn out to be the most promising optimizer and is followed by SMS-EMOA, NSGA-III, NSGA-II, and MOEA/D-DE.

As in the non-parametric statistical study of the hypervolume indicator, the Wilcoxon test is used to determine significant differences between samples obtained from the binary C-metric comparisons. Table VIII shows the results of this test and alternatives in boldface are the winners of each comparison. In this, again the metric-driven optimizers show to have the best performance. From Table VIII, HV-MODE achieves the maximum number of wins and is followed by SMS-EMOA, NSGA-II, NSGA-III and MOEA/D-DE.

Additionally, a multi-comparative test of Friedman among optimizers is presented in the supplementary materials.

Finally, it is important to mention that for a real application with an FBM prototype, is necessary to perform the online optimization of the control system in real-time. The above requires the selection of adequate implementation technologies to reduce the optimizer search time. In this way, efficient optimizers are more suitable for narrow time windows. Considering T_a as the average time required by the most efficient optimizer to find the Pareto front approximation, the computational efficiencies of compared optimizers are listed from best to worst: T_a for MOEA/D-DE, $1.1 \cdot T_a$ for NSGA-II, $1.6 \cdot T_a$ for NSGA-III, $1.8 \cdot T_a$ for HV-MODE, and $3.7 \cdot T_a$ for SMS-EMOA.

VI. Conclusions

The proposed adaptive controller tuning strategy shows to be effective for speed control of the FBM. Despite the highly non-linear dynamic behavior of this system and the induced highly non-linear uncertainties, the proposed strategy can find an accurate estimated model online to tune the parameters of the PD-computed torque controller that reduces the speed regulation error while produces a smooth control action that prevents the mechanism wear.

From the control engineering point of view, the adaptive controller tuning strategies based on the metric-driven approach achieve the best performances. The ACTS-SMS-EMOA obtains the lowest speed regulation error (i.e., ACTS-SMS-EMOA finds the most suitable GFBM dynamic parameters used in the speed controller) while the ACTS-HV-MODE develops the smoothest control signal. The above according to the control performance indicators IAE, ITAE, ISE, ITSE, and IADU.

TABLE IV: Results of ACTS-NSGA-II, ACTS-MOEA/D-DE, ACTS-SMS-EMOA, ACTS-HV-MODE and ACTS-NSGA-III.

Alternative	IAE	ITAE	ISE	ITSE	IADU
ACTS-NSGA-II	0.1139	0.3201	0.0042	0.0120	0.4931
ACTS-MOEA/D-DE	0.1239	0.3382	0.0102	0.0279	0.6351
ACTS-SMS-EMOA	**0.0946**	**0.2661**	**0.0030**	**0.0086**	0.4817
ACTS-HV-MODE	0.1256	0.3555	0.0060	0.0175	**0.4274**
ACTS-NSGA-III	0.1005	0.2780	0.0066	0.0179	0.6100
PI controller	1.6932	4.6533	0.8132	0.8192	0.4167

Based on statistical evidence over the hypervolume indicator, the best search approaches considering the disturbed system are provided by metric-driven and hybrid alternatives (SMS-EMOA, HV-MODE, and NSGA-III). These are followed in performance by the dominance-based alternative (NSGA-II), which finds Pareto front approximations whose solutions have low values of the estimation error objective. Concerning to decomposition based approach (MOEA/D-DE), the lack of diversity and convergence of the found trade-offs diminishes the overall control system performance.

According to the C-metric, statistical evidence shows that the metric-driven optimizers (HV-MODE and SMS-EMOA) find better non-dominated solutions than the rest of the alternatives. It is important to highlight that the metric-driven alternatives achieve a better coverage than dominance-based, hybrid, and decomposition-based approaches.

The proposed metric-driven HV-MODE shows outstanding performance when compared with the other optimizers regarding the two selected indicators (hypervolume indicator and C-metric). The above is due to the inclusion of elitism by using an external archive to store the most promising solutions. Additionally, the knowledge share of the best-known solutions in this archive (according to their hypervolume contribution) and the currently found solutions in population, allows guiding the search for alternatives in less explored regions of the Pareto front. On the other hand, the interchange between the evolutionary operations of the variants DE/current-to-rand/1/bin and DE/current-to-pbest/1/bin enhances the exploration and exploitation capabilities of HV-MODE when necessary. These evolutionary operations can be modified to extrapolate the use of HV-MODE to different problems.

Among the observed advantages of the online multi-objective meta-heuristic optimization approach to adaptive tuning methods, is the possibility to include preferences to improve the performance of one or more tuning criteria based on the application necessities (these can also be changed dynamically). Then, as further work is the inclusion of progressive or interactive preferences that depend on the problem context, for example, giving a lower preference to the control action smoothness when abrupt uncertainties are identified.

Acknowledgements

The first author acknowledges the support from the Consejo Nacional de Ciencia y Tecnología (CONACyT) through the scholarship to pursue his graduate studies at CIDETEC-IPN.

TABLE V: Statistical results of the hypervolume metric (HV).

Optimizer	Mean	Std
NSGA-II	0.1917	0.2797
MOEA/D-DE	0.3448	0.4381
HV-MODE	0.0392	0.0769
SMS-EMOA	0.1705	0.2798
NSGA-III	0.0837	0.1957

TABLE VI: Wilcoxon test results of the hypervolume metric (HV).

Test	R_+	R_-	*p-value*
HV-MODE vs MOEA/D-DE	408826	80729	+1.8083e-74
HV-MODE vs NSGA-II	401456	88099	+4.3119e-68
HV-MODE vs NSGA-III	257657	231898	=0.1517
HV-MODE vs SMS-EMOA	375305	114250	+8.2065e-48
MOEA/D-DE vs **NSGA-II**	190007	299548	-1.0909e-09
MOEA/D-DE vs **NSGA-III**	90369	399186	-3.4695e-66
MOEA/D-DE vs **SMS-EMOA**	168805	316800	-1.1759e-16
NSGA-II vs **NSGA-III**	124212	365343	-4.7425e-41
NSGA-II vs **SMS-EMOA**	217084	272471	-0.0020
NSGA-III vs SMS-EMOA	343907	145648	+2.6682e-28

TABLE VII: Statistical results of the two-set-coverage metric (C-metric).

Comparison	Mean	Std
NSGA-II vs MOEA/D-DE	0.3972	0.4611
MOEA/D-DE vs NSGA-II	0.3345	0.3783
NSGA-II vs HV-MODE	0.2045	0.3292
HV-MODE vs NSGA-II	0.6792	0.3890
NSGA-II vs SMS-EMOA	0.3339	0.4343
SMS-EMOA vs NSGA-II	0.4667	0.4042
NSGA-II vs NSGA-III	0.3106	0.4567
NSGA-III vs NSGA-II	0.3251	0.3621
MOEA/D-DE vs HV-MODE	0.1445	0.2666
HV-MODE vs MOEA/D-DE	0.6915	0.4450
MOEA/D-DE vs SMS-EMOA	0.3029	0.4075
SMS-EMOA vs MOEA/D-DE	0.5319	0.4772
MOEA/D-DE vs NSGA-III	0.2172	0.4024
NSGA-III vs MOEA/D-DE	0.3081	0.3923
HV-MODE vs SMS-EMOA	0.6416	0.4446
SMS-EMOA vs HV-MODE	0.2352	0.3317
HV-MODE vs NSGA-III	0.5620	0.4830
NSGA-III vs HV-MODE	0.1696	0.2662
SMS-EMOA vs NSGA-III	0.3911	0.4772
NSGA-III vs SMS-EMOA	0.2804	0.3630

TABLE VIII: Wilcoxon test results of the two-set-coverage metric (C-metric).

Test	R_+	R_-	*p-value*
NSGA-II vs NSGA-III	206085	159855	+0.0012
HV-MODE vs SMS-EMOA	413232	74346	+5.1037e-83
HV-MODE vs NSGA-III	384280	83748	+1.3327e-69
HV-MODE vs NSGA-II	402703.5	86851.5	+2.3806e-69
NSGA-III vs **SMS-EMOA**	140938.5	252002.5	-1.3637e-13
MOEA/D-DE vs **SMS-EMOA**	143376	340260	-3.3295e-30
NSGA-II vs SMS-EMOA	227468.5	236697.5	=0.5921
MOEA/D-DE vs **NSGA-II**	175280	290815	-1.9110e-11
MOEA/D-DE vs NSGA-III	102916	115875	=0.1802
HV-MODE vs MOEA/D-DE	437604.5	44066.5	+2.7528e-117

The second and third authors acknowledge the support from the CONACyT through the projects No. 182298 and No. 220522, respectively. The second and fourth authors acknowledge the support of the Secretaría de Investigación y Posgrado (SIP) through the projects No. SIP-20180196 and No. SIP-20180637, respectively.

References

[1] G. Incerti, "On the dynamic behaviour of a four-bar linkage driven by a velocity controlled dc motor," *International Journal of Mechanical, Aerospace, Industrial, Mechatronic and Manufacturing Engineering*, vol. 6, no. 9, pp. 1895 – 1901, 2012.

[2] W. Shang and S. Cong, "Nonlinear computed torque control for a high-speed planar parallel manipulator," *Mechatronics*, vol. 19, no. 6, pp. 987 – 992, 2009.

[3] S. Boyd, C. Baratt, and S. Norman, "Linear controller design: limits of performance via convex optimization," *Proceedings of the IEEE*, vol. 78, no. 3, pp. 529–574, Mar 1990.

[4] M. G. Villarreal-Cervantes and J. Alvarez-Gallegos, "Off-line pid control tuning for a planar parallel robot using de variants," *Expert Syst. Appl.*, vol. 64, no. C, pp. 444–454, Dec. 2016.

[5] A. E. Ruano, S. S. Ge, T. M. Guerra, F. L. Lewis, J. C. Principe, and M. Colnarič, "Computational intelligence in control," *Annual Reviews in Control*, vol. 38, no. 2, pp. 233 – 242, 2014.

[6] R. E. King, *Computational Intelligence in Control Engineering*. New York, NY, USA: Marcel Dekker, Inc., 1999.

[7] E.-G. Talbi, *Metaheuristics: From Design to Implementation*. Wiley Publishing, 2009.

[8] G. Reynoso-Meza, X. Blasco, J. Sanchis, and M. Martínez, "Controller tuning using evolutionary multi-objective optimisation: current trends and applications," *Control Engineering Practice*, vol. 28, pp. 58–73, 2014.

[9] H. V. H. Ayala and L. dos Santos Coelho, "Tuning of pid controller based on a multiobjective genetic algorithm applied to a robotic manipulator," *Expert Systems with Applications*, vol. 39, no. 10, pp. 8968 – 8974, 2012.

[10] K. Deb, A. Pratap, S. Agarwal, and T. Meyarivan, "A fast and elitist multiobjective genetic algorithm: NSGA-II," *IEEE Transactions on Evolutionary Computation*, vol. 6, no. 2, pp. 182–197, 2002.

[11] J. Kennedy and R. Eberhart, "Particle swarm optimization," in *Proceedings of ICNN'95 - International Conference on Neural Networks*, vol. 4, Nov 1995, pp. 1942–1948 vol.4.

[12] M. Mahmoodabadi, M. Taherkhorsandi, and A. Bagheri, "Optimal robust sliding mode tracking control of a biped robot based on ingenious multi-objective pso," *Neurocomputing*, vol. 124, pp. 194 – 209, 2014.

[13] A. Shenfield and P. J. Fleming, "Multi-objective evolutionary design of robust controllers on the grid," *IFAC Proceedings Volumes*, vol. 44, no. 1, pp. 14 711 – 14 716, 2011, 18th IFAC World Congress.

[14] C. M. Fonseca and P. J. Fleming, "Genetic algorithms for multiobjective optimization: Formulationdiscussion and generalization," in *Proceedings of the 5th International Conference on Genetic Algorithms*. San Francisco, CA, USA: Morgan Kaufmann Publishers Inc., 1993, pp. 416–423.

[15] R. Storn and K. Price, "Differential evolution – a simple and efficient heuristic for global optimization over continuous spaces," *Journal of Global Optimization*, vol. 11, no. 4, pp. 341–359, Dec 1997.

[16] I. B. Tijani, R. Akmeliawati, A. G. A. Muthalif, and A. Legowo, "Optimization of pid controller for flexible link system using a pareto-based multi-objective differential (pmode) evolution," in *2011 4th International Conference on Mechatronics (ICOM)*, May 2011, pp. 1–6.

[17] P. Stewart, D. Stone, and P. Fleming, "Design of robust fuzzy-logic control systems by multi-objective evolutionary methods with hardware in the loop," *Engineering Applications of Artificial Intelligence*, vol. 17, no. 3, pp. 275 – 284, 2004.

[18] C. J. Wu, T. L. Lee, Y. Y. Fu, and L. C. Lai, "Auto-tuning fuzzy pid control of a pendubot system," in *2007 IEEE International Conference on Mechatronics*, May 2007, pp. 1–6.

[19] D. E. Goldberg, *Genetic Algorithms in Search, Optimization and Machine Learning*, 1st ed. Boston, MA, USA: Addison-Wesley Longman Publishing Co., Inc., 1989.

[20] G.-Q. Zeng, J. Chen, Y.-X. Dai, L.-M. Li, C.-W. Zheng, and M.-R. Chen, "Design of fractional order pid controller for automatic regulator voltage system based on multi-objective extremal optimization," *Neurocomputing*, vol. 160, pp. 173 – 184, 2015.

[21] H. Wang, G. Zeng, Y. Dai, D. Bi, J. Sun, and X. Xie, "Design of a fractional order frequency pid controller for an islanded microgrid: A multi-objective extremal optimization method," *Energies*, vol. 10, no. 10, 2017.

[22] M. G. Villarreal-Cervantes, A. Rodríguez-Molina, C. V. García-Mendoza, O. Peñaloza-Mejía, and G. Sepúlveda-Cervantes, "Multi-objective on-line optimization approach for the dc motor controller

tuning using differential evolution," *IEEE Access*, vol. 5, pp. 20 393–20 407, 2017.
[23] C. A. C. Coello, G. B. Lamont, and D. A. V. Veldhuizen, *Evolutionary Algorithms for Solving Multi-Objective Problems (Genetic and Evolutionary Computation)*. Secaucus, NJ, USA: Springer-Verlag New York, Inc., 2006.
[24] K. Li, K. Deb, Q. Zhang, and S. Kwong, "An evolutionary many-objective optimization algorithm based on dominance and decomposition," *IEEE Transactions on Evolutionary Computation*, vol. 19, no. 5, pp. 694–716, Oct 2015.
[25] N. Beume, B. Naujoks, and M. Emmerich, "Sms-emoa: Multiobjective selection based on dominated hypervolume," *European Journal of Operational Research*, vol. 181, no. 3, pp. 1653 – 1669, 2007.
[26] S. Jiang, Y. S. Ong, J. Zhang, and L. Feng, "Consistencies and contradictions of performance metrics in multiobjective optimization," *IEEE Transactions on Cybernetics*, vol. 44, no. 12, pp. 2391–2404, Dec 2014.
[27] I. Landau, R. Lozano, and M. M'Saad, *Adaptive Control: Algorithms, Analysis and Applications*. New York, NY, USA: Springer Science+Business Media, 2011.
[28] Z. Song, J. Yi, D. Zhao, and X. Li, "A computed torque controller for uncertain robotic manipulator systems: Fuzzy approach," *Fuzzy Sets and Systems*, vol. 154, no. 2, pp. 208 – 226, 2005.
[29] D. W. Corne and J. D. Knowles, "No free lunch and free leftovers theorems for multiobjective optimisation problems," in *Proceedings of the 2Nd International Conference on Evolutionary Multi-criterion Optimization*, ser. EMO'03. Berlin, Heidelberg: Springer-Verlag, 2003, pp. 327–341.
[30] Q. Zhang and H. Li, "Moea/d: A multiobjective evolutionary algorithm based on decomposition," *IEEE Transactions on Evolutionary Computation*, vol. 11, no. 6, pp. 712–731, Dec 2007.
[31] K. Price, R. M. Storn, and J. A. Lampinen, *Differential Evolution: A Practical Approach to Global Optimization (Natural Computing Series)*. Secaucus, NJ, USA: Springer-Verlag New York, Inc., 2005.
[32] J. Zhang and A. C. Sanderson, "Jade: Adaptive differential evolution with optional external archive," *IEEE Transactions on Evolutionary Computation*, vol. 13, no. 5, pp. 945–958, Oct 2009.
[33] E. n. Mezura-Montes, J. Velázquez-Reyes, and C. A. Coello Coello, "A comparative study of differential evolution variants for global optimization," in *Proceedings of the 8th Annual Conference on Genetic and Evolutionary Computation*, ser. GECCO '06, 2006.
[34] K. Deb, "An efficient constraint handling method for genetic algorithms," *Computer Methods in Applied Mechanics and Engineering*, vol. 186, no. 2, pp. 311 – 338, 2000.
[35] K. Deb and H. Jain, "An evolutionary many-objective optimization algorithm using reference-point-based nondominated sorting approach, part i: Solving problems with box constraints," *IEEE Transactions on Evolutionary Computation*, vol. 18, no. 4, pp. 577–601, Aug 2014.
[36] H. Jain and K. Deb, "An evolutionary many-objective optimization algorithm using reference-point based nondominated sorting approach, part ii: Handling constraints and extending to an adaptive approach," *IEEE Transactions on Evolutionary Computation*, vol. 18, no. 4, pp. 602–622, Aug 2014.
[37] H. Li and Q. Zhang, "Multiobjective optimization problems with complicated pareto sets, moea/d and nsga-ii," *IEEE Transactions on Evolutionary Computation*, vol. 13, no. 2, pp. 284–302, April 2009.
[38] E. Mezura-Montes, M. Reyes-Sierra, and C. A. C. Coello, *Multi-objective Optimization Using Differential Evolution: A Survey of the State-of-the-Art*. Berlin, Heidelberg: Springer Berlin Heidelberg, 2008, pp. 173–196.
[39] W. C. Schultz and V. C. Rideout, "Control system performance measures: Past, present, and future," *IRE Transactions on Automatic Control*, vol. AC-6, no. 1, pp. 22–35, Feb 1961.
[40] G. Reynoso-Meza, J. Sanchis, X. Blasco, and M. Martínez, "Preference driven multi-objective optimization design procedure for industrial controller tuning," *Information Sciences*, vol. 339, pp. 108 – 131, 2016.
[41] T.-C. Chen and T.-T. Sheu, "Model reference neural network controller for induction motor speed control," *IEEE Transactions on Energy Conversion*, vol. 17, no. 2, pp. 157–163, Jun 2002.

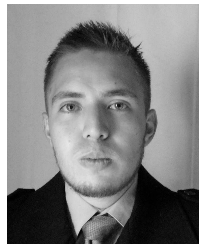

Alejandro Rodríguez-Molina received the B. S. degree in computer systems engineering from the National Polytechnic Institute (IPN) in 2013 and the M.Sc. in computer science from the Center for Research and Advanced Studies of the National Polytechnic Institute (CINVESTAV-IPN) in 2015. He is currently a Ph.D. candidate in robotic and mechatronic systems engineering at the Center for Innovation and Technological Development in Computing of the National Polytechnic Institute (CIDETEC-IPN). He is interested in the design and implementation of bio-inspired meta-heuristics for optimization and their application to engineering problems.

Miguel G. Villarreal-Cervantes received the B. S. degree in electronics engineering from the Veracruz Technologic Institute in 2003 and the M. Sc. and Ph. D. degrees in electrical engineering from the Center for Research and Advanced Studies CINVESTAV, Mexico in 2005 and 2010, respectively. He is Full Professor at the Postgraduate Department in the "Centro de Innovación y Desarrollo Tecnológico en Cómputo" of the Instituto Politécnico Nacional (CIDETEC-IPN). He is member of National System of Researchers (S.N.I.) and of the Expert Network on Robotics and Mechatronics of the IPN (ENRM-IPN) in Mexico. He was the head of both the mechatronic section in CIDETEC-IPN during 2013-2016 and the ENRM-IPN during 2012-2017. His research interests include mechatronic design based on optimization (mono and multi-objective optimization), bio-inspired metaheuristics in the optimal mechatronic design, optimal tuning for the mechatronic system control based on metaheuristic algorithms (offline and online strategies) and robotics.

Efrén Mezura-Montes Efrén Mezura-Montes was born in Xalapa, México, in 1973. He received the diploma degree in computer systems engineering from the University of the Americas, Puebla, in 1997, the M.Sc. degree in artificial intelligence from the University of Veracruz in 2001, and the Ph.D. degree in computer science from the Center for Research and Advanced Studies of the National Polytechnic Institute (CINVESTAV-IPN) in 2004. He has published over 110 papers in peer-reviewed journals and conferences. His research interests are in the design, study, and application of nature-inspired meta-heuristic algorithms to solve complex optimization problems. He is currently the head of the Ph.D. graduate program in artificial intelligence of the Artificial Intelligence Research Center, University of Veracruz. He is also a member of the IEEE Computational Intelligence Society Evolutionary Computation Technical Committee and the IEEE Systems, Man and Cybernetics Society Soft Computing Technical Committee. He is also a member of the Mexican National Researchers System Level 2 and a regular member of the Mexican Computing Academy.

Mario Aldape-Pérez Mario Aldape-Pérez received his Ph.D. in Computer Science from the National Polytechnic Institute of Mexico, in 2011. He is a Professor of Computer Architecture at CIDETEC of the National Polytechnic Institute of Mexico. His current research interests include Associative Memories, Soft Computing and FPGA Implementation of High Performance Pattern Classification algorithms. Dr. Aldape-Pérez is a member of the IEEE Computer Society and the ACM. He was President of the Academy of Digital Systems at the School of Computing of the National Polytechnic Institute of Mexico during 2011-2013. He was Head of Research and Technology Innovation Department in CIDETEC during 2013-2016. Since 2016 he is the Academic Deputy Director of CIDETEC.

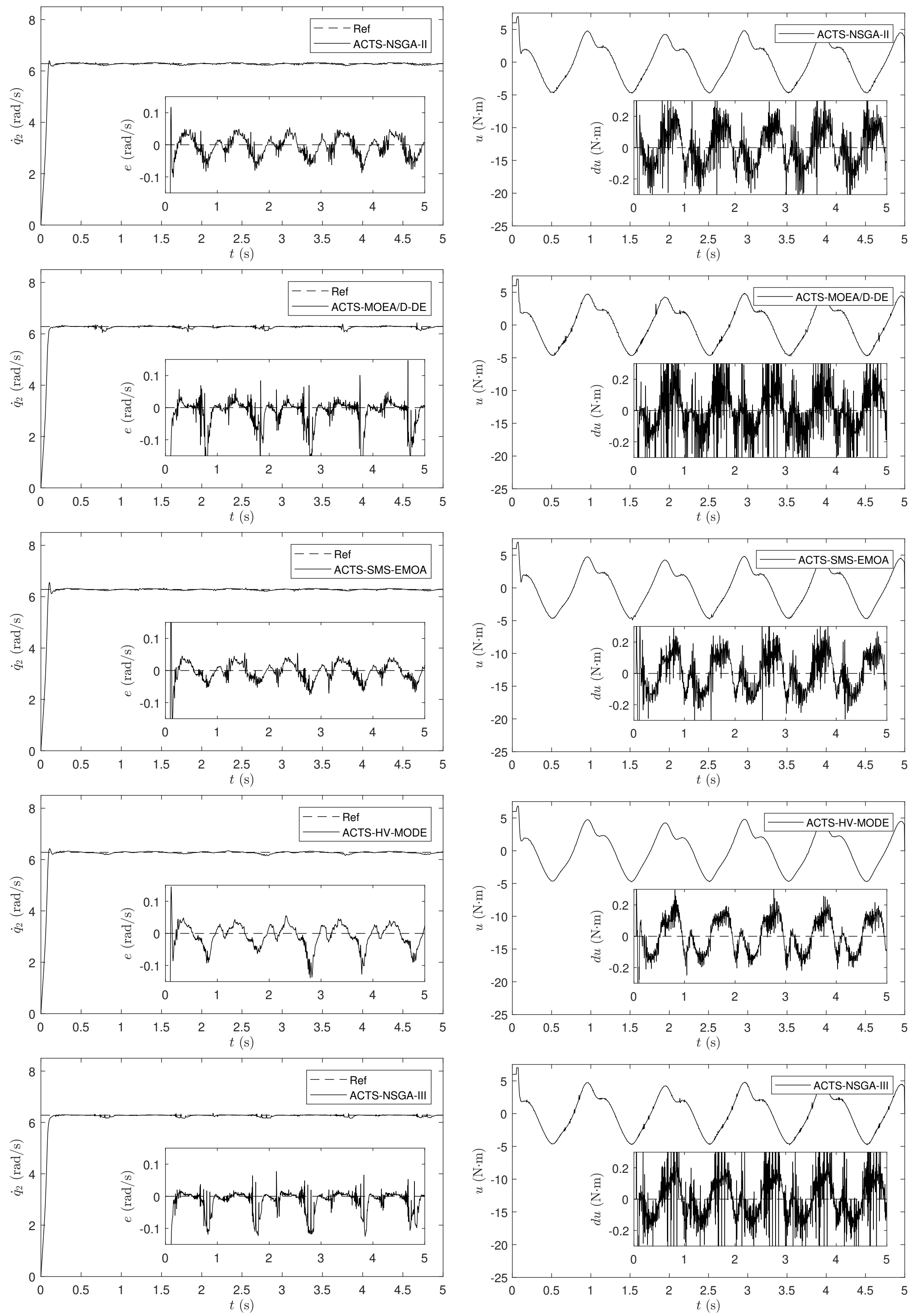

Fig. 5: Behavior of ACTS-NSGA-II, ACTS-MOEA/D-DE, ACTS-HV-MODE, ACTS-SMS-EMOA and ACTS-NSGA-III.